Thin-film composite hollow fiber membranes incorporated with graphene oxide in polyethersulfone support layers for enhanced osmotic power density

Myoung Jun Park[a], Sungil Lim[a], Ralph Rolly Gonzales[a], Sherub Phuntsho[a], Dong Suk Han[b], Ahmed Abdel-Wahab[c], Samer Adham[d], Ho Kyong Shon[a]*

[a]*Centre for Technology in Water and Wastewater, School of Civil and Environmental Engineering, University of Technology Sydney (UTS), P.O. Box 123, 15 Broadway, NSW 2007, Australia*

[b]*Center for Advanced Materials, Qatar University, P.O. Box 2713, Doha, Qatar*

[c]*Chemical Engineering Program, Texas A&M University at Qatar, PO, Box 23874, Doha, Qatar*

[d]*Global Water Sustainability Center, ConocoPhillips Water Technology Ltd., P.O. Box 24750, Doha, Qatar*

*Corresponding author: Ho Kyong Shon; Email: hokyong.shon-1@uts.edu.au;

Tel.: +61 2 9514 2629; Fax: +61 2 9514 2633.

Abstract

This study focused on the development of pressure retarded osmosis (PRO) thin film composite (TFC) membranes for enhanced osmotic power using hollow fiber polyethersulfone (PES) support structure modified by incorporating hydrophilic graphene oxide (GO) nanosheets. The GO loadings in the hollow fiber substrates were varied to improve water flux performances without compromising the mechanical strength. GO embedded (≤0.2 wt%) PES hollow fiber supports revealed noticeable improvements in pure water permeability, improved structural morphologies, as well as the hydrophilicity within the support layer, without deteriorating the mechanical properties. The GO (0.2 wt%)-incorporated TFC-PRO membrane appeared to have an initial PRO flux (without any applied pressure) of 43.74 L m^{-2} h^{-1}, lower specific reverse salt flux of 0.04 g L^{-1} and structural parameter (S) of 522 μm, significantly better than the control membrane. The maximum power density of 14.6 W m^{-2} was achieved at an operating pressure of 16.5 bar under the condition of DI water and 1 M NaCl as feed and draw solutions, respectively. The results obtained in this study indicate that modification of PRO hollow fiber support layer by incorporating nanoparticles such as GO nanosheet can be a useful tool to improve the PRO performance.

1. Introduction

The global demand for clean and renewable energy has significantly increased in recent years due to serious air pollution and global warming caused by the current fossil fuel-based energy sources. Fossil fuels are non-renewable and the depletion of the available energy resources are eminent. Thus, the utilization of renewable sources of energy such as wind, solar, tide, biomass, and geothermal energy has gained growing interest recently [1-3]. Osmotic energy from salinity gradient using pressure retarded osmosis (PRO) has shown to have great potential for providing sustainable resources [2, 4].

The PRO process utilizes the osmotic pressure difference between two solutions of different salinities, where water from the solution of less salt concentration passes through a selectively permeable membrane to the concentrated solution by natural osmotic process [5]. The osmotic energy obtained from the PRO process is then converted into mechanical energy and electricity using a hydro turbine and generator, respectively. With efficient engineering design, PRO process can obtain high power density, which allows it to efficiently draw free energy from the high salinity solutions present naturaly or created artificially [6, 7]. PRO is currently one of the promising applications for harvesting renewable energy from mixing of fresh and saline waters. However, several challenges still remain before the osmotic power by PRO process becomes commercially viable and one of the major challenges is the lack of suitable membranes tailored for the PRO process.

In recent years, many studies have been conducted on developing PRO membranes to make the process viable for commercial applications. PRO membranes should have characteristics very similar to the membranes used for forward osmosis (FO) process. The ideal FO or PRO membranes should have high water flux, low concentration polarization (CP) in the membrane support, high porosity, hydrophilicity, thin selective layer, and low structural parameter (S).

68 However, unlike the FO process, PRO is operated at high pressure and hence requires

69 membranes with high mechanical properties that can withstand high hydraulic pressures during

70 the PRO operation [8, 9]. Like any other thin film composite (TFC)-based membranes, the

71 PRO membrane support layers are fabricated either as a flat type or hollow fiber configuration

72 via phase separation technique while the thin polyamide (PA) selective layer is formed by

73 interfacial polymerization (IP) method [10, 11]. This typical two-step process forms a TFC

74 membrane that has a wide range of applications for various separation processes.

75 In previous studies, various types of membrane supports for TFC-PRO membrane were

76 introduced, such as electrospun nanofiber membrane [12, 13], flat-sheet membrane [14-17] and

77 hollow fiber membrane [8, 18-24]. Reverse osmosis (RO) membranes made of TFC flat-sheet

78 membranes have been most widely used in desalination and water purification. The

79 commercially available TFC membrane modules are usually manufactured as a spiral wound

80 type. However, the spiral wound flat-sheet TFC membrane modules are observed to be less

81 suitable for PRO applications because of high fouling propensity and severe membrane

82 deformation by the spacers [25, 26]. However, TFC hollow fiber membrane modules could be

83 more suitable for the PRO process because the hollow fiber is self-supporting membrane and,

84 hence, spacer-free. Besides, hollow fiber membrane modules can have much higher packing

85 density as compared to the spiral wound membrane modules [18, 21, 23, 27]. Though, TFC-

86 PRO hollow fiber membrane itself should have high mechanical properties to be able to

87 withstand high hydraulic pressures for achieving high power density which is the product of

88 water flux and the applied hydraulic pressure. The power density has been reported to reach a

89 maximum theoretical value when the applied hydraulic pressure is equal to half of the osmotic

90 pressure difference across the membrane. For example, when seawater is used as draw solution

91 and fresh water as feed solution, a theoretical osmotic pressure of draw solution is ≈ 27 bar and

92 an half of that pressure (13 ~ 14 bar) would be required at draw side to achieve the maximum

93 power density. Due to this reason, a mechanically strong hollow fiber membrane is an

94 important factor for the feasible application of PRO process. Therefore, recent studies on

95 developing TFC-PRO hollow fiber membrane have been focused on designing robust

96 membrane materials via various fiber spinning techniques, different polymers, and spinning

97 conditions [8, 19-21, 23, 28].

98 In our previous studies on the development of FO membranes, we used graphene oxide (GO)

99 as filler for the membrane substrates in the fabrication of flat-sheet TFC-FO membranes, and

100 found that the FO performance was significantly improved by lowering the S value at a suitable

101 GO loading rate without significantly compromising its mechanical properties [29, 30]. Due to

102 its typical characteristics such as atomic thicknesses of 1-2 nm with a two-dimensional single

103 layer and hydrophilic properties with the presence of hydrophilic functional groups, the GO

104 nanosheet offers high potential for fabricating composite polymeric membranes with improved

105 structural properties, high hydrophilicity, and excellent antifouling propensity [29, 31-35].

106 Despite the significant improvement in the TFC-FO membranes performance obtained with

107 nanomaterials incorporation, the fabrication of mixed matrix hollow fiber support for TFC-

108 PRO membranes has yet to be fully explored. Thus, in this study, we investigated the

109 fabrication of high performance TFC-PRO membrane by incorporating hydrophilic GO

110 nanosheets in the hollow fiber substrate.

111 The main objective of the study is to investigate the potential of GO-incorporated hollow fiber-

112 support membranes for improving the PRO performance. Three different TFC-PRO

113 membranes were prepared and their performances were compared in terms of water flux and

114 osmotic power density. The effects of GO incorporation on the mechanical stability against

115 hydraulic pressure were systematically evaluated by determining membrane burst pressure for

116 both membrane support and active layers. In addition, the effect of pre-stabilization of the PA

selective layer and transport properties of TFC hollow fiber membranes were invistegated. Intrinsic membrane properties such as porosity, pore size, hydrophilicity, permeability, selectivity and mechanical properties were comparatively evaluated.

2. Experimental

2.1 Materials

Polyethersulfone (PES, Veradel® 3000P, Mw = 62,000 ~ 64,000 g/mol), provided from Solvay Specialty Polymers, Republic of Korea, was used as the polymer material. For hollow fiber support membrane preparation, n-methyl-2-pyrrolidone (NMP, Merck) was employed to dissolve the PES polymer, while polyethylene glycol 400 (PEG, Mw = 400 g/mol, Merck) was used as an additive. Hollow fiber membrane post-treatment was conducted using a Glycerol (99.5%) from Chem-Supply Pty. Ltd. (Australia). PA layer formation was performed using trimesoyl chloride (TMC, 98%), 1,3-phenylenediamine (MPD, 99%) and sodium dodecyl sulfate (SDS, ≥99.0%) purchased from Sigma-Aldrich. Hexane (99.9%) from Merck was used as an organic solvent for dissolving TMC. Polyethylene glycol (PEG) and polyethylene oxide (PEO) with various molecular weights purchased from Sigma-Aldrich and were used for measuring pore size distributions. Graphene oxide (GO) nanosheets used in this study was prepared via modified Hummer's method [36, 37] that was reported in our previous study [29].

2.2 Hollow fiber membrane support preparation

Dope solution compositions and spinning parameters for the preparation of hollow fiber membrane substrates are presented in Table 1. Three different hollow fiber membrane supports

139 were prepared in this study. A digital stirring machine, with constant speed of 800 rpm at 80

140 ℃ for 12 h, was used to mix a certain amount of PES with NMP as a solvent, and PEG and GO

141 as additives, in a two-neck glass reactor. The dope solutions were then cooled down in room

142 temperature with continuous stirring for another 12 h, transferred into a syringe pump and then

143 degassed for 24 h at room temperature prior to hollow fiber spinning. To evaluate the effects

144 of GO addition in the membrane supports, a control substrate without GO addition was

145 prepared and denoted as HF-0. For the preparation of GO-incorporated dope solutions,

146 different loadings of GO in NMP were sonicated for homogeneous dispersion prior to addition

147 of PES and PEG. According to the GO loadings with respect to PES amounts (weight ratio to

148 the PES), hollow fiber supports were denoted as HF-GO-0.1 and HF-GO-0.2 which contain 0.1

149 and 0.2 wt% GO, respectively.

150 Table 1. Spinning parameters of hollow fiber support membranes prepared

| Spinning parameter	Hollow fiber supports		
Sample code	HF-0	HF-GO-0.1	HF-GO-0.2
Dope solution composition (wt%)	PES/PEG/NMP (20/40/40)	PES/PEG/NMP (20/40/40)	PES/PEG/NMP (21/39.5/39.5)
GO loadings in polymer (wt%)	0	0.1	0.2
Bore solution	DI water		
Outer solution	Pure NMP		
Dope flow rate (ml/min)	1.8		
Bore flow rate (ml/min)	1.2		
Outer flow rate (ml/min)	0.2		
Air gap distance (cm)	1.0		
Winding speed (m/min)	2.2		
Coagulation bath	Tap water		

151

152 The hollow fiber membranes with highly porous structure to the outer surface were fabricated

153 using a triple nozzle (Fig. S1a) and hollow fiber spinning machine (Fig. S2) with a wet-wet

154 spinning process. As demonstrated in Fig. 1, DI water, polymer dope, and pure NMP were

155   separately supplied into the bore, inner, and outer channels, respectively, of the triple spinneret

156   spinning machine design [38-41]. Basically, outer surface of membranes was designed to be

157   highly porous and open pore structure via a pure NMP extrusion into the outer channel for

158   reducing the ICP effect through faster solvent transport during PRO process. The solutions

159   were simultaneously extruded and immediately immersed in coagulation water bath with an air

160   gap distance of 1 cm to solidify the polymer. The as-spun samples were collected by a drum

161   type winder with an almost free fall condition (take-up speed: 2.2 m/min). All parameters were

162   set at the same conditions except the dope solution compositions as shown in Table 1.

163   Fabricated hollow fiber membranes were then kept in tap water for 48 h and soaked in

164   water/glycerol (50/50 wt%) aqueous solution for another 48 h for post-treatment. Subsequently,

165   the hollow fiber samples were dried in the air for membrane modulation. For membrane

166   performance tests, hollow fibers were modulated by assembling 5 fibers (effective length: 13 -

167   14 cm), as shown in Fig. S3 (A). The prepared samples were used for evaluating membrane

168   performances.

169
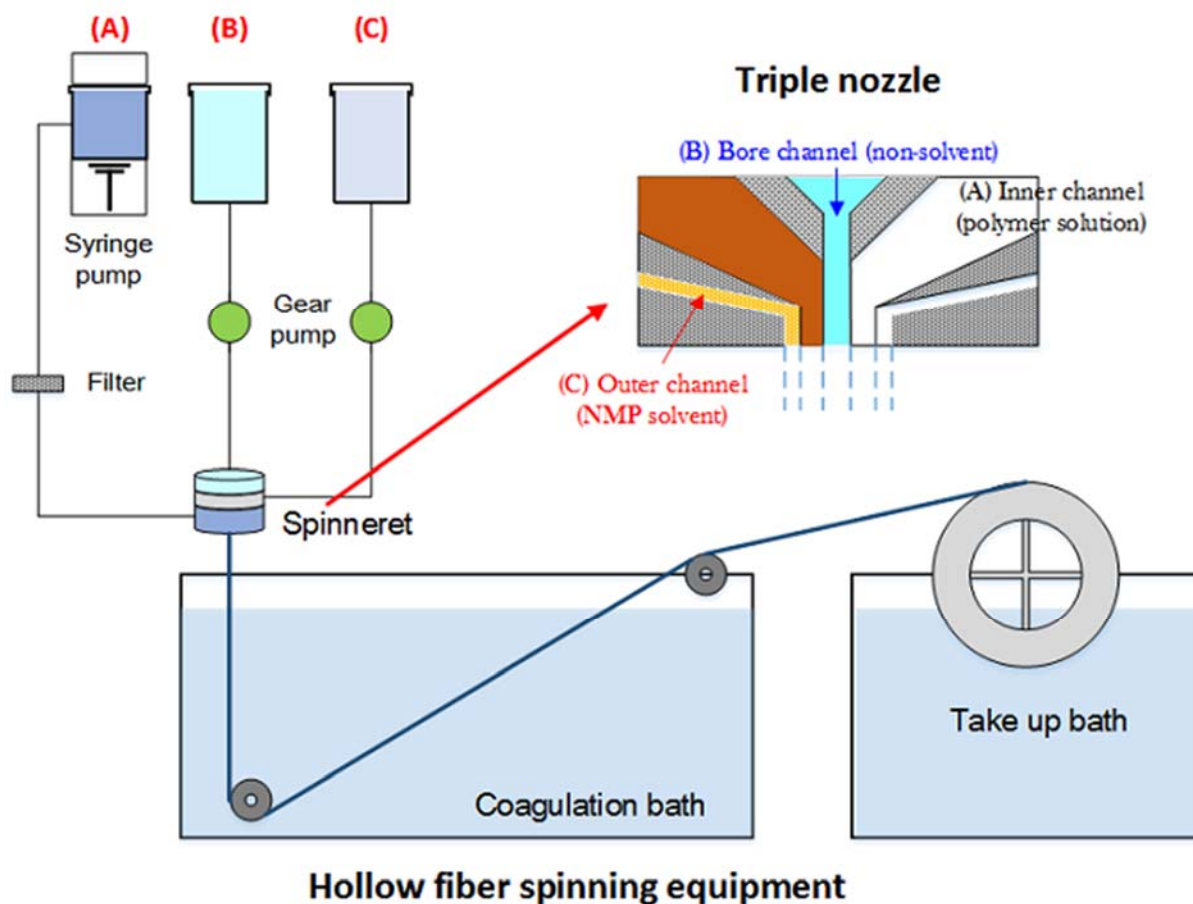
Fig. 1. Schematic diagram of hollow fiber spinning set-up. (A) polymer dope solution, (B) bore solution, (C) pure NMP

2.3 IP process onto the lumen side of membrane supports

Fig. S3 illustrates the IP process of membrane samples, during which a PA active layer was formed on the inner surface of hollow fibers. First, the inlet side (lumen side) of vertically-held membrane module was connected to the peristaltic pump with silicone tube to introduce an aqueous solution (2 wt% MPD + 0.1 wt% SDS solution) with a flow rate of 4.1 mL/min for 3 min. N_2 gas purging was then employed at a pressure of 100 kPa for 5 min to remove the excess solution. To complete the IP reaction, TMC (0.15 wt%) in hexane was introduced with a flow rate of 2.3 mL/min for 5 min to provide enough time to react with residual MPD. Finally, the

182 unreacted TMC was removed by purging N_2 gas (100 kPa) for 30s. All membrane modules

183 were then soaked in deionized (DI) water without further treatment, and kept in cool condition

184 prior to performance experiments and membrane characterizations. According to the sample

185 codes of hollow fiber supports, the PA layer deposited samples were denoted from the HF-0,

186 HF-GO-0.1 and HF-GO-0.2 to the THF-0, THF-GO-0.1 and THF-GO-0.2, respectively.

187

2.4. Characterization of hollow fiber membranes

189 The morphological properties and surface roughness of as-spun membranes were characterized

190 by field emission scanning electron microscope (FE-SEM) and atomic force microscopy (AFM)

191 images, respectively, and more analysis details can be found in our previous study [29].

192 Mechanical properties of hollow fiber supports were obtained by an Advanced Testing System

193 (LS1, Lloyd instruments Ltd, UK) with a load cell of 1 kN. A pair of wire grip with bollard

194 and vice clamp (Max. 2 kN) was selected to hold hollow fiber samples. Gauge length, pre-load

195 and cross-head speed were set as 80 mm, 0.05 N and 30 mm/min, respectively. Inner diameter

196 (ID) and outer diameter (OD) of hollow fiber membrane supports were determined by a digital

197 microscope (Max. magnification ratio: × 500) to obtain the cross sectional area (mm^2) of

198 samples. Hydrophilic property of membrane surface was evaluated by an optical tensiometer

199 (Theta Lite 100) and contact angle values were estimated using an image processing software.

200 Membrane support pore properties such as mean pore size and pore size distribution were

201 obtained from solute transport experiment using PEG and PEO as feed solutions and the

202 procedure is described in Supplementary Information.

203 Hollow fiber membrane porosity (ε) was calculated by Eq. (1) [8]. Wet samples of 5 cm in

204 length (l, cm) were cut and then dried in a dry oven at 100 °C for 12 h, and placed in a desiccator

205   for another 12 h to completely remove any remaining water from the samples. The dried

206   membranes were weighed (m, g) with 5 fibers for each measurement.

207     $$\varepsilon = \frac{\frac{1}{4}\pi l \rho_p \left(OD^2 - ID^2\right) - m}{\frac{1}{4}\pi l \rho_p \left(OD^2 - ID^2\right)} \times 100\% \qquad (1)$$

208   where ρ_p, OD and ID are the PES polymer density (1.37 g cm^{-3}), outer fiber diameter (m), and

209   inner fiber diameter (m), respectively. All characterization methods were performed at least

210   five times.

211

2.5. RO performance and burst pressure evaluation for membrane supports and TFC membranes

213

214   *2.5.1. Pure water permeability and burst pressure evaluations for hollow fiber supports*

215   Pure water permeability (*PWP*, L m^{-2} h^{-1} bar^{-1}) and burst pressure (bar) of hollow fiber

216   supports were determined using a lab scale membrane test device that is illustrated in Fig. S4.

217   DI water was constantly circulated for both the inner and the outer sides of the hollow fiber

218   module (flow rate: 150 mL/min). Prior to the measurement of weight changes to the permeate

219   side, the tested samples were stabilized at the applied trans-membrane pressure (from lumen to

220   shell side) of 1 bar for 1 h. The *PWP* was calculated using the Eq. (2) and (3)

221     $$J_w = \frac{\Delta V}{A_m \cdot \Delta t} \qquad (2)$$

222     $$PWP(A) = \frac{J_w}{\Delta P} \qquad (3)$$

where J_w, ΔV (L), A_m and Δt (h) is the water flux (L m^{-2} h^{-1}), permeate volume, effective membrane area (lumen side, m^2) and sampling time, respectively, in Eq. (2), and ΔP in Eq. (3) is the trans-membrane pressure difference (bar).

Afterwards, the pressure in the lumen side was gradually increased in increments of 2 to 3 bar until the membranes exhibited a complete burst. The *PWP* at each pressure was measured by averaging the data collected for 20 min.

2.5.2. Evaluation of intrinsic properties and burst pressures of the TFC-PRO membranes

To determine the burst pressure (or critical pressure) and RO performances for TFC-PRO membranes, an experiment was performed for hollow fiber supports (section 2.5.1) and was also conducted using the PRO unit (Fig. S4). Evaluation of the burst pressures for TFC-PRO membranes was performed without any membrane compaction. Initial pressure of 5 bar was applied with the DI water to the lumen side at flow rate of 150 mL/min, stabilized for 20 min, and the average *PWP* was determined. Then, the pressure was increased at 2 bar increments until the pressure reached to 13 bar while being stabilized for 20 min at each pressure and then it was increased by 1 bar per increment until the membrane breakage occurred within 20 min and the membrane breakage pressure was defined as 'burst pressure'. In addition, the 'critical point' at certain pressures for TFC-PRO membranes was also determined where the membranes started to generate considerable deformation and damage determined by the sudden increase of water permeability.

Intrinsic properties, such as *A* value and salt rejection (*R*, %) for TFC-PRO membranes were evaluated at two different operation conditions. First, prepared TFC-PRO membranes were pre-stabilized at 8 bar for 1 h, and then the *A* value was determined via collecting permeated pure water and *R* value was obtained from the rejection rate of 2000 ppm NaCl when the feed

246 water was operated at 8 bar. Conductivity and volume changes of the permeated water as well

247 as applied pressures were monitored and recorded by a conductivity meter and data auto-

248 logging system. The R value and salt permeability (B) was calculated using Eq. (4) and Eq. (5),

249 respectively [42].

250 $$R = \left(1 - \frac{C_p}{C_f}\right) \times 100\%$$ (4)

251 $$B = \frac{1-R}{R}(\Delta P - \Delta \pi)A$$ (5)

252 where C_f and C_p in Eq. (4) are the salt concentrations of the feed and permeate solutions,

253 respectively, and $\Delta\pi$ in Eq. (5) the osmotic pressure difference across the membrane.

254   Alternatively, the TFC-PRO samples for THF-0, THF-GO-0.1 and THF-GO-0.2 were pre-

255 stabilized for 1 h below their critical points which were found to be at 13.5 bar, 13.5 bar and

256 16.5 bar, respectively, prior to performance evaluation. This was followed by determination of

257 A and R values of samples at different pressures. The critical point for each membrane was

258 determined from the results of RO mode operations at variously applied pressures. The

259 temperature of all solutions was maintained at $23 \pm 1^{\circ}$C during the tests.

260

261 ***2.6. PRO performance evaluation for TFC-PRO membranes***

262   The PRO performance of the TFC membranes was determined as circulating a draw solution

263 (DS, 1.0 M NaCl) of 5 L to the hollow fiber lumen side (facing active layer) and a feed solution

264 (FS, DI water) of 2 L to the shell side using the PRO unit. The flow rate was set for both streams

265 at 150 mL/min. Before conducting PRO evaluations, the TFC-PRO membranes of THF-0,

266 THF-GO-0.1 and THF-GO-0.2 were stabilized for 1 h at 13.5 bar, 13.5 bar and 16.5 bar,

267   respectively, of which pressures are below the critical points of each membrane. After the

268   membrane stabilization, each sample was tested from 0 bar stepwise up to the stabilized

269   pressures and this test was denoted as the first run (1st-run). In order to confirm the stability

270   and reproducibility of each tested samples, the second (2nd-run) operation was conducted right

271   after the first run at the same ranges of applied pressures. The PRO water flux was calculated

272   using Eq. (4). The reverse salt flux (J_s, g m^{-2} h^{-1}) was determined by Eq. (6) as follows:

273   $$J_s = \frac{\Delta(C_t V_t)}{A_m \cdot \Delta t}$$ (6)

274   where C_t and V_t are the changes of salt concentration and the feed volume at time interval (Δt),

275   respectively.

276   The power density (W, W m^{-2}) can be obtained from Eq. (7) where ΔP is the pressure

277   difference across the TFC-PRO membrane.

278   $$W = J_w \Delta P$$ (7)

279   Detailed information on determining S values for fabricated TFC membranes are indicated in

280   the Supplementary Information (Section 1.2).

281

282   **3. Results and discussion**

283   *3.1. Morphological properties of hollow fiber supports*

284   The effect of GO loadings on the morphological changes of PES hollow fiber membrane

285   supports was characterized by FE-SEM analysis as indicated in Fig. 2 which reveals the inner

286   and outer surfaces as well as the cross-section of all prepared samples for HF-0, HF-GO-0.1

287   and HF-GO-0.2. A typical asymmetric structure with finger-like and sponge-like structures

appeared in the cross-section of all membranes. In the case of outer surface, all membranes revealed a sponge-like structure with highly porous and rough surface without skin-layers formation. This is because the co-extrusion of pure NMP (solvent) in the outer fluid channel during spinning likely induced a delayed demixing [8, 18, 23, 43]. In contrast, due to the fast phase inversion induced by strong non-solvent (water) as a bore fluid, relatively dense skin-layers with small pores were formed on the inner surface of all the prepared hollow fiber membrane supports. The simultaneous extrusion of three different solutions via triple spinneret also subsequently induced the formation of dual-layered structure in the cross-section: 1) the finger-like structures are dominantly formed near the lumen side of hollow fiber membranes due to the faster demixing by the water as bore fluid, and 2) the less finger-like but more sponge-like structures appeared as close to the outer surface because the NMP solvent as the outer channel strongly influenced to a slower phase inversion from out to inward [18].

Interestingly, it can be clearly distinguished from the cross-section SEM images that the number of macrovoid structures increased with an increase in GO loadings. As the GO loadings increased from 0 to 0.2 wt%, the density and length of finger-like pores increased at the internal zone of the hollow fibers near the membrane lumen. Furthermore, the number of outward-pointed macrovoids increased instead of sponge-like structure at the outer region. This trend was also observed in our previous studies [29, 30] and other studies [44, 45] in which GO was incorporated in the polymeric membrane substrates. Low loading rates of GO with uniform dispersion in the dope solution increase the thermodynamic incompatibility between polymer and solvent due to the hydrophilicity of the nanomaterial. Thus, the hydrophilic GO enhanced the exchange rate between the solvent and non-solvent during the phase inversion which resulted in hindrance of sponge-like structure formation [29, 46]. It can be noted that more finger-like morphologies were obtained for HF-GO-0.2 against HF-GO-0.1. The polymer concentration increase from 20 to 21 wt% and the GO concentration increase for HF-GO-0.2

may both have increased the dope solution viscosity, but only 0.1 wt% increase of GO loading seemed to predominantly affect the phase separation kinetics than the polymer solution viscosity [21].
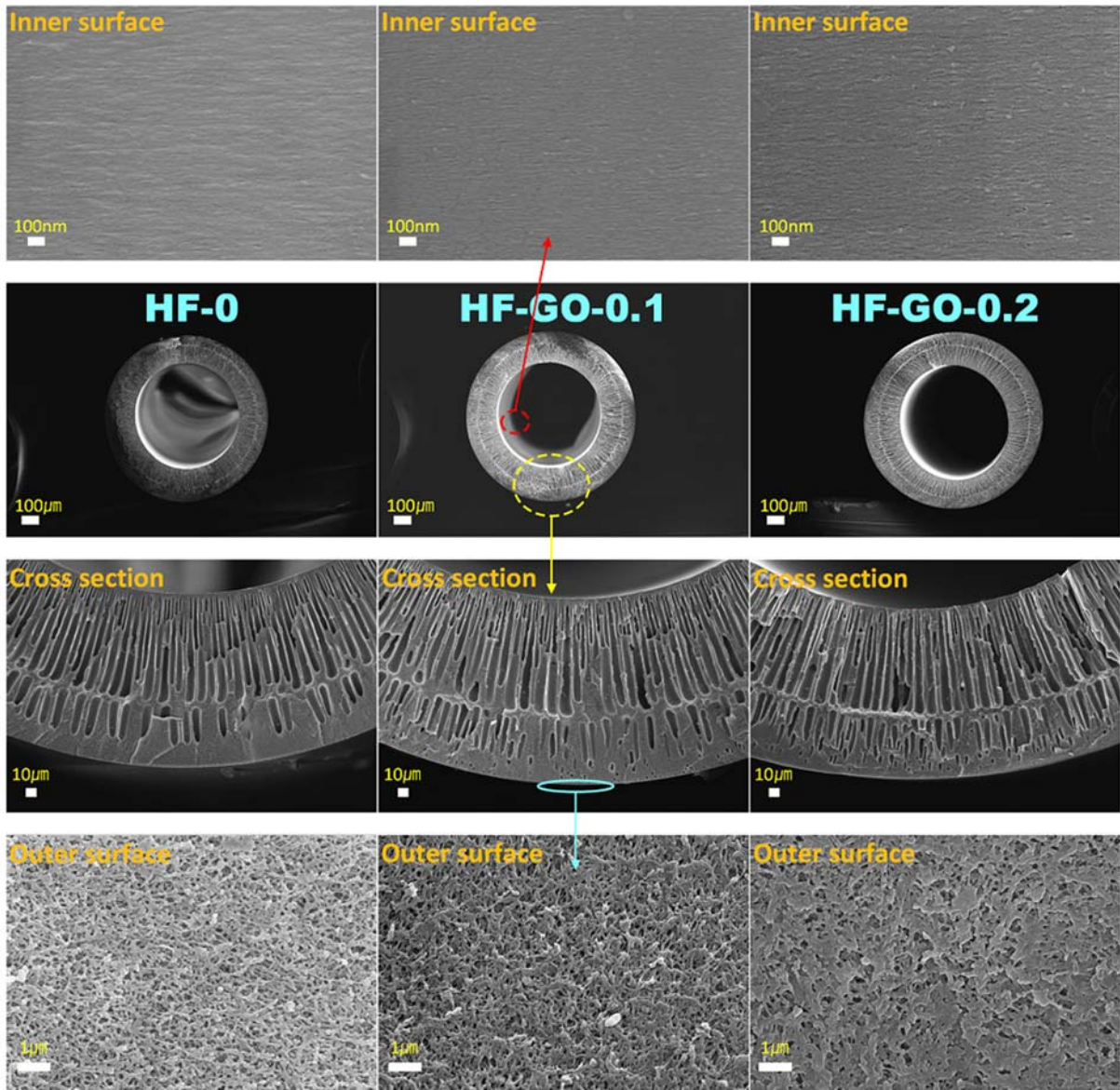
Fig. 2. FE-SEM images of as-spun hollow fiber supports (HF-0, HF-GO-0.1 and HF-GO-0.2).

320 The presence and incorporation of GO in the hollow fiber substrates were confirmed by

321 photographs and SEM images from Fig. S1(b) and Fig. S5, respectively. After incorporation

322 of GO in PES substrates, the color of hollow fiber surfaces has become darker from off-white

323 to brownish gray as GO loadings increased as shown in Fig. S1(b). The presence of GO in the

324 PES substrates also observed in the cross-section of SEM images (Fig. S5) as red circles for

325 HF-GO-0.1 and HF-GO-0.2 indicate some GO aggregation. Although assumed not significant,

326 some GO nanoparticles might likely aggregate even though the GO loadings were small (≤ 0.2

327 wt%), which is due to the high dope solution viscosity increased by high polymer concentration

328 of 20-21 wt% and the high content of PEG as an additive [29, 46]. However, this minor GO

329 aggregation in the membrane substrates did not cause deterioration of mechanical properties.

330

331 *3.2. Effect of GO loading on the characteristics of hollow fiber supports*

332 Table 2 summarizes the physical properties of fabricated hollow fiber supports. The tensile

333 strength and the elongation at break for HF-0 were 5.18 MPa and 47.37 %, respectively, and

334 incorporation of 0.1 wt% GO (HF-GO-0.1) did not alter these values significantly. Thus, it can

335 be concluded that the mechanical properties of the PES support were not affected by a small

336 amount of GO incorporation. In fact, the tensile strength of HF-GO-0.2 slightly increased to

337 5.56 MPa although this might not be due to increased GO loading (0.2 wt%) only but also

338 likely due to the increase of polymer concentration.

339

340   Table 2. Hollow fiber sizes, mechanical properties, *PWP* and pore size properties of prepared
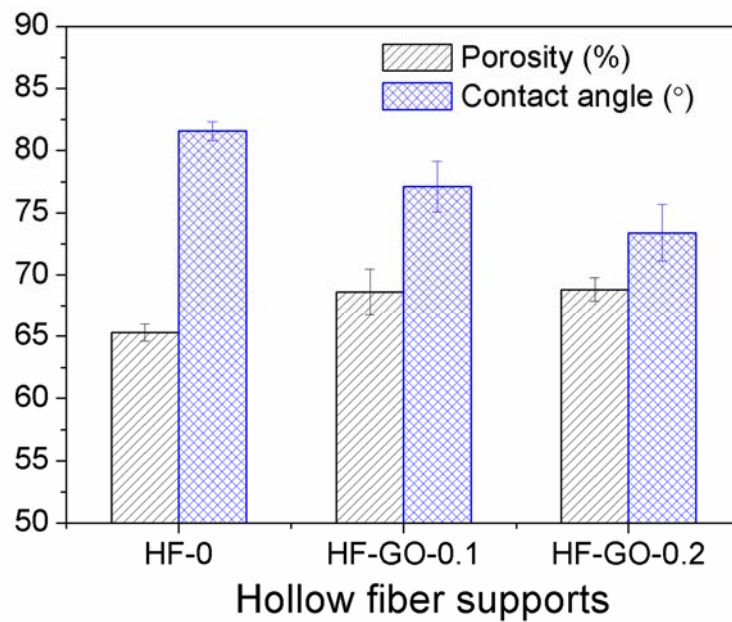
341   hollow fiber supports.

Membrane properties	Hollow fiber supports		
	HF-0	HF-GO-0.1	HF-GO-0.2
ID/OD (µm)	663/1050	664/1044	685/1070
Thickness (µm)	196	190	193
Tensile strength (MPa)	5.18 ± 0.14	5.20 ± 0.21	5.56 ± 0.20
Elongation at break (%)	47.37 ± 4.52	46.96 ± 4.16	46.36 ± 3.16
Toughness[1] (N m^{-2})	2.50 ± 0.12	2.53 ± 0.15	3.08 ± 0.09
PWP (L m^{-2} h^{-1} bar^{-1})	322	361	387
Mean pore diameter, μ_p (nm)	8.28	8.85	9.03
Geometric standard deviation, σ_p	1.86	1.90	1.94

342   [1] Toughness was calculated by obtaining the intergral underneath the stress-strain curve.

343

344   The mean pore diameter and *PWP* of hollow fiber supports are presented in Table 2. Without

345   GO incorporation, the HF-0 showed the mean pore diameter of 8.28 nm, however, it

346   continuously increased as GO loadings increased to HF-GO-0.1 and HF-GO-0.2 with the mean

347   pore diameter of 8.85 nm and 9.03 nm, respectively. This increase in pore diameter is a result

348   of hydrophilic GO effect that accelerated the rate of the phase inversion and induced the

349   increase of lumen surface pores, as shown in the cross-section images (Fig. 2), and the

350   reduction of membrane thickness (Table 2). The *PWP* results also revealed a consistent trend

351   with the pore size of the hollow fiber supports. GO embedded in PES supports at 0.1 and 0.2

352   wt% loading noticeably improved the *PWP* to 361 and 387 L m^{-2} h^{-1} bar^{-1}, respectively, as

353   compared to that of HF-0 (322 L m^{-2} h^{-1} bar^{-1}). The enhanced *PWP* could be not only due to

354   enhanced membrane porosity but also due to improved surface hydrophilicity by GO addition

355   [31, 32]. This enhanced hydrophilicity is evident from Fig. 3 where the contact angle decreased

356   correspondingly with an increase of GO content. The contact angle of HF-0 was 81.6° which

357   decreased to 77.13° at 0.1 wt% GO loading and further to 73.41° at 0.2 wt% GO loading. GO

358 is known to contain abundant hydroxyl, carboxyl and epoxy functional groups which may

359 improve hydrophilicity by decreasing surface energy of the membrane surface. Similar results

360 were reported from previous studies where GO was used as a filler of composite membranes

361 [29, 32, 44, 45, 47, 48].

363 Fig. 3. Membrane porosity and contact angle of as-spun hollow fiber supports.

364

365 Fig. 3 show that the overall porosity of membranes increased from 65.3% to 68.6% with 0.1

366 wt% GO loading while this increase to 68.8% was very marginal at 0.2 wt% GO loading. This

367 is probably due to the effect of higher polymer concentration of dope solution that produced

368 denser matrix of overall membrane structure although the membrane morphology of HF-GO-

369 0.2 in the cross-section of SEM image seemed more porous than that of HF-GO-0.1.

370
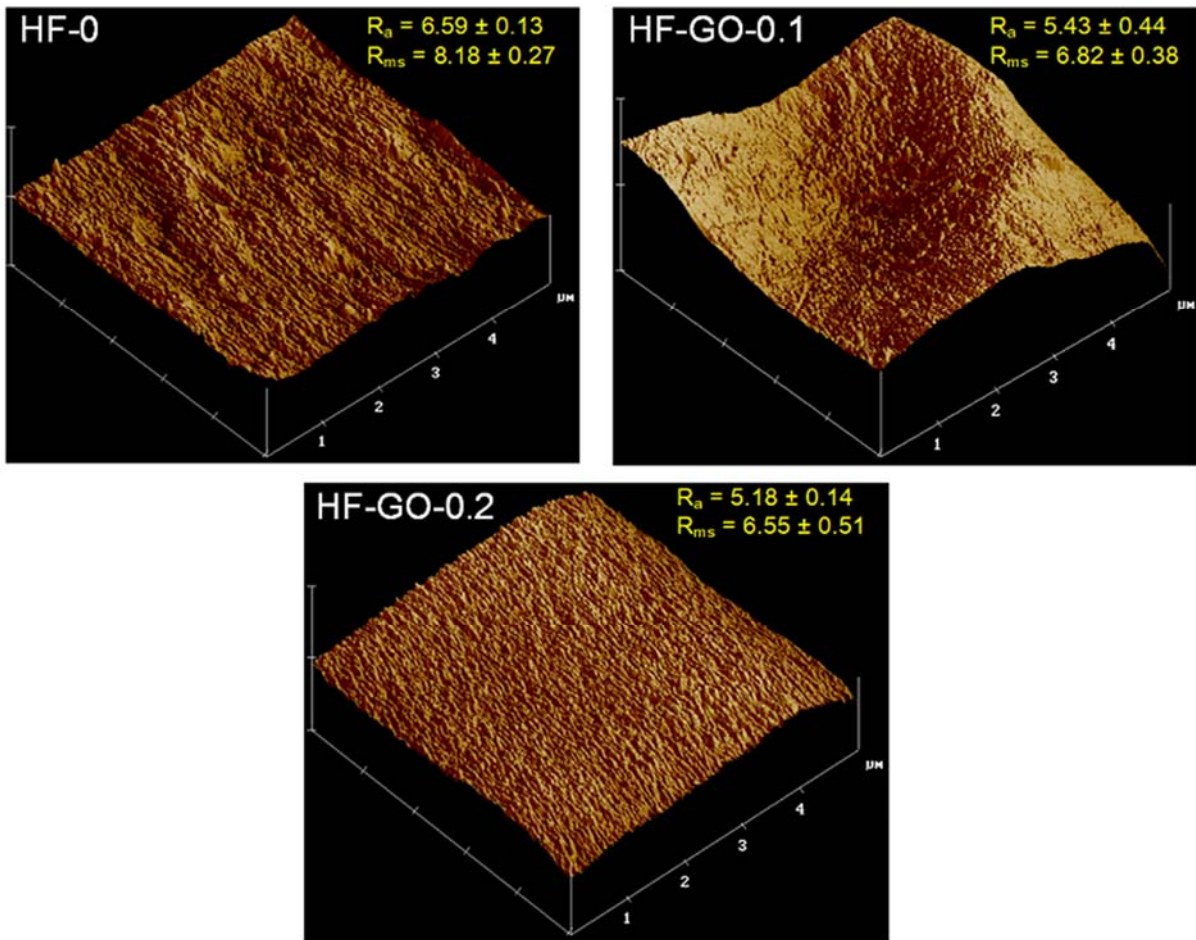
Fig. 4. AFM images of inner surface of hollow fiber supports for HF-0, HF-GO-0.1 and HF-GO-0.2.

373

The surface morphology or roughness of the lumen side of the prepared hollow fiber membranes was characterized using AFM analysis. Fig. 4 shows the three-dimensional (3D) AFM images of the membrane lumen surfaces for HF-0, HF-GO-0.1 and HF-GO-0.2. Additionally, the mean roughness (R_a, nm) and root mean square ridge elevation (R_{ms}, nm) obtained from averaging the values from five images are presented in the images. The R_a and the R_{ms} of HF-0 were 6.59 nm and 8.18 nm, respectively. However, the R_a and the R_{ms} values for HF-GO-0.1 and HF-GO-0.2 membrane samples were relatively lower due to GO incorporation. The AFM images also show the uniform and smoother surface morphologies for

HF-GO-0.1 and HF-GO-0.2 membrane samples, which are likely a result of well-dispersed GO in the PES substrate [29, 44, 45, 49].

3.3. Morphology and membrane stability evaluation of TFC-PRO membranes

The successful depositions of PA layer on the inner surface of hollow fiber membranes were confirmed by FE-SEM observation as depicted in Fig. 5. The top surface of PA layer for hollow fiber samples was shown on the left-side images of Fig. 5 (a, b, and c) and the images on the right (d, e, and f) show the cross-section at near the inner surface of hollow fiber. The typical ridge-and-valley structures were seen on the membrane surfaces for all prepared TFC membranes from the SEM images, which affirms the presence of well-formed thin film of PA layer via interfacial IP process [18, 19, 21]. From the cross-sectional SEM images of TFC-PRO membranes, interestingly, the average thickness (averaged from the ten randomly measured) of PA layers has significantly decreased in the order of 269 nm, 181 nm and 163 nm for THF-0, THF-GO-0.1 and THF-GO-0.2, respectively.

Similar tendency was experienced in previous studies which reported that the relatively smaller pore size (Table 2) for pure PES support may have caused the MPD monomer to stay at the mouth of the membrane pores, and rapidly diffuse into the organic phase and then react with TMC during the IP [8, 50]. Moreover, rougher surface morphology (Fig. 4) may cause the MPD with non-uniformly filled-up on the membrane surface. Therefore, this characteristic of the membrane surface in the IP reaction is a result of the relatively thick, rough and ineffective formation of PA layer [8, 51, 52]. The membrane surface with larger pore size and smoother surface, but with hydrophilic property formed by GO incorporation may prove to be the more favourable conditions for the regular deposition of thin MPD layer prior to the IP reaction. Consequently, this induces the formation of homogeneous PA selective layer with thinner and

406 defect-free PA deposition [29]. It is evident that THF-GO-0.2 had the thinnest PA layer among

407 the three prepared samples, which consisted of the characteristics of the biggest surface pore

408 but lowest roughness and strong hydrophilicity. Similar trend was also observed in the

409 literature [53].
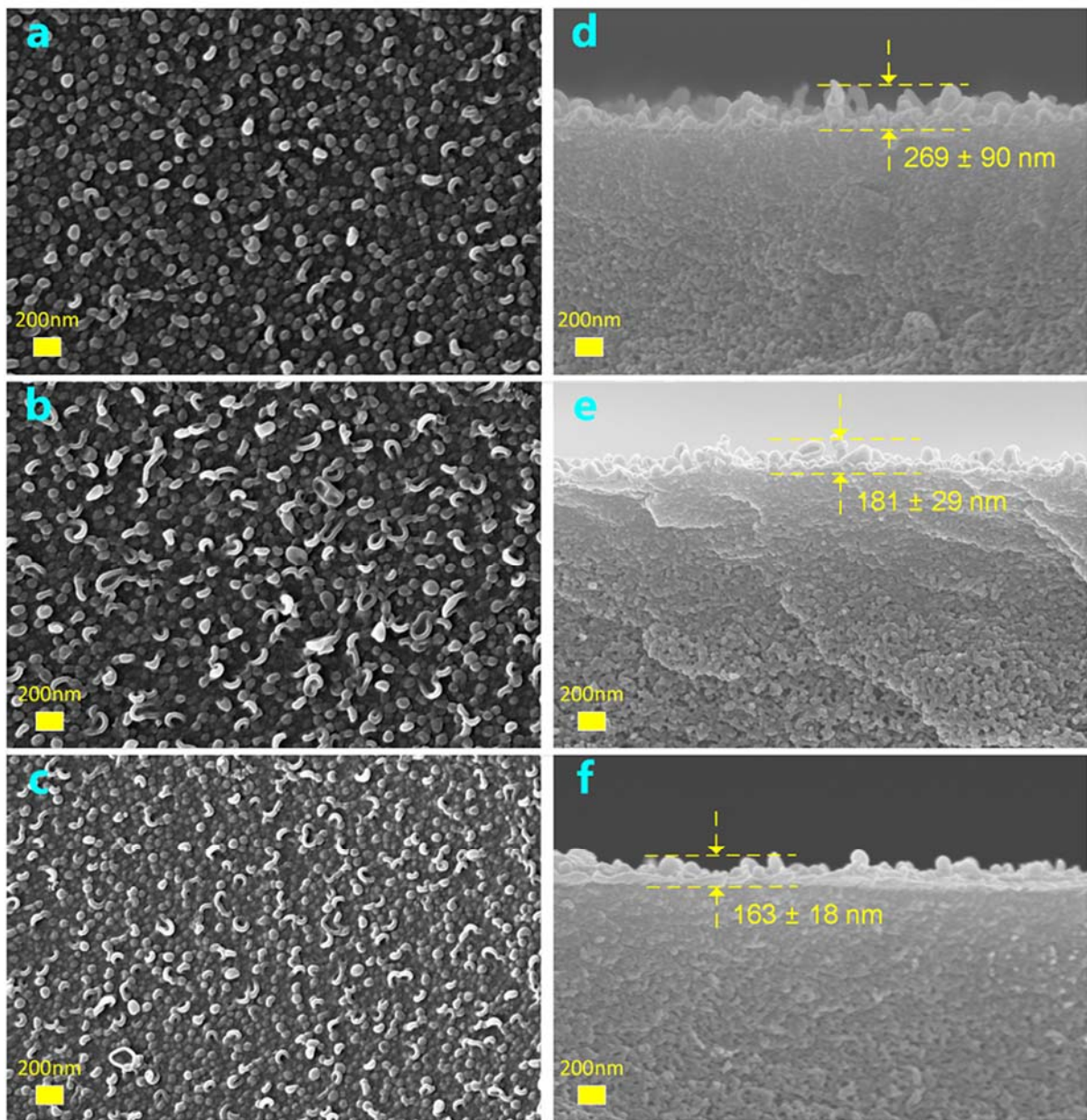
410

411 Fig. 5. PA active layer top and cross-section images near to the PA layer of THF-0 (a and d),

412 THF-GO-0.1 (b and e) and THF-GO-0.2 (c and f) characterized by FE-SEM.

Evaluation of membrane stability and determination of their maximum ability against high hydraulic pressure are very important especially for TFC-PRO hollow fiber membranes, in which the active layer (PA layer) is deposited on the lumen surface of the hollow fiber. This is because the application of the high hydraulic pressures from inside to outside will induce physical stress resulting in an expansion of membrane inner (lumen) diameter, and considerably affect the integrity of PA layer due to deformation [18]. Therefore, the TFC-PRO hollow fiber membranes should possess strong mechanical properties to withstand against hydraulic pressure on the lumen side, otherwise the hollow fiber membrane may burst especially when the pressure exceeds its critical pressure. Polymeric membranes in general without any support materials have limitations with its mechanical properties [54]. For the long-term performance stability of the membrane with minimum membrane damage, the robustness of the fabricated membranes should be evaluated and this was done by determining the burst pressure and the critical point of each hollow fiber membrane sample [18, 21, 23, 54].

The burst pressure of the hollow fiber supports and TFC-PRO membranes was tested based on their *PWP* at increasing hydraulic pressure as indicated in Fig. 6. The normalized *PWP* (Fig. 6(a)) for all hollow fiber supports indicated a rapid reduction in the *PWP* values with the increase of applied pressures up to somewhat mainly due to membrane compaction [21]. There was about 30% decrease of the *PWP* for HF-0 at 13.9 bar and then suddenly increased when the membrane deformation starts, until the membrane is completely burst at 16.3 bar. Similar pattern was also observed with HF-GO-0.1 membrane sample with a burst pressure of 16.2 bar. Meanwhile, the highest burst pressure of 18.6 bar was observed for HF-GO-0.2 membrane however, this same membrane sample also showed the most severe reduction rate in normalized *PWP* which was then followed by HF-GO-0.1 and HF-0. This may be related with the pore sizes of the hollow fiber supports (Table 2) which follows the order of HF-GO-0.2 >

437 HF-GO-0.1 > HF-0. The larger pores and higher surface porosities of the membranes likely

438 results in more compaction of the membrane.

439 In contrast to the normalized PWP trend, all TFC-PRO membranes showed a gradual increase

440 in PWP with the increase in applied pressures (Fig. 6 (b)). This phenomenon may be the result

441 of the following two effects: (1) the increase of membrane effective area attributed by the

442 stretching and thinning of the PA layer, and (2) the reduced water transport resistance due to

443 the decreased membrane thickness, when the hydraulic pressure is applied to the membrane

444 lumen side [9, 18, 21]. The steady increase of A values for TFC-PRO membranes was observed

445 up to the point of critical pressures of around 14 bar for HF-0 and HF-GO-0.1, and 17.3 bar for

446 HF-GO-0.2. At pressures above the critical pressure, a sudden increase of A values was

447 observed until the membranes reached complete failure (burst) at around 16.0 bar for both

448 THF-0 and THF-GO-0.1, and 18.8 bar for THF-GO-0.1. These findings indicate that the

449 damage of PA layer by irreversible changes or minor defects, will be experienced before

450 reaching the burst pressure of hollow fiber support layer, where the support layer deformation

451 begins with significant increase of PWP from Fig. 6 (a) and Fig. 6 (b) [18].

452 The evaluation of mechanical stability of the hollow fiber membranes showed that addition of

453 0.1 wt% GO into PES hollow fiber support layer did not undermine the overall mechanical

454 stabilities compared to pure PES support. However, the hollow fiber membrane whose PES

455 concentration was increased by 1 wt% polymer with 0.2 wt% GO incorporation, showed

456 significant improvement in mechanical stability, even though this membrane was observed to

457 have more macrovoids and higher porosity (Fig. 2) compared to the other membranes.

458 Membrane toughness, which was determined by integrating the stress-strain curve as listed in

459 Table 2, further confirms the robustness of these fabricated membranes. The highest membrane

460 toughness of 3.08 N m^{-2} was obtained for HF-GO-0.2 while the HF-0 (2.50 N m^{-2}) and HF-

461   GO-0.1 (2.53 N m^{-2}) showed similar toughness. This trend was consistent with the results from

462   the robustness tests (Fig. 6) and the mechanical strength (Table 2). Overall, the HF-GO-0.2

463   membrane sample showed desirable characteristic of the membrane support for TFC-PRO

464   membrane with improved hydrophilicity and porosity, and best mechanical properties, while

465   exhibiting the lowest surface roughness amongst all the samples prepared in this study.

466
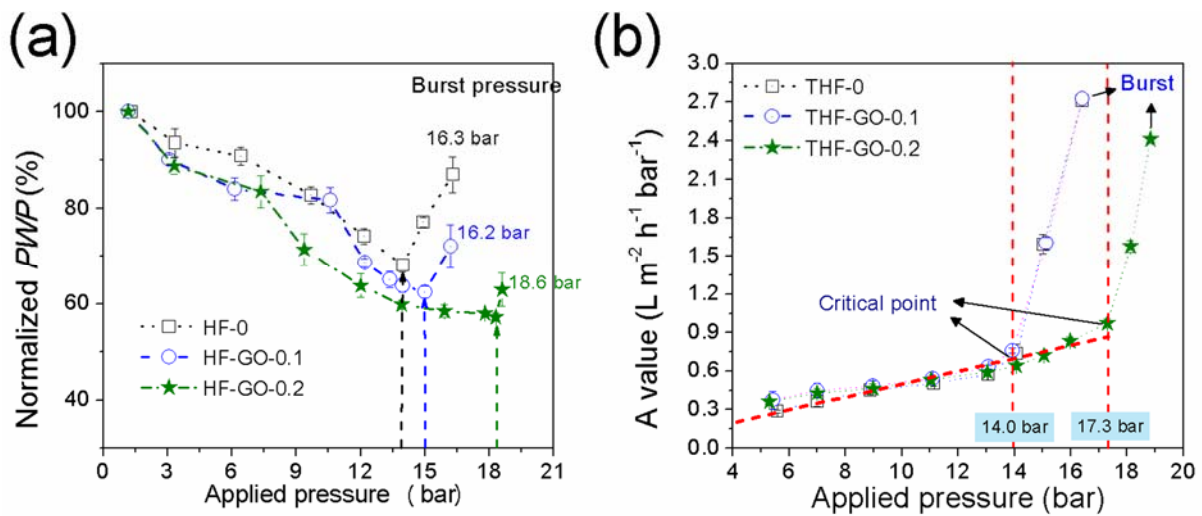
468   Fig. 6. (a) Normalized *PWP* (%) of HF-0, HF-GO-0.1 and HF-GO-0.2 and (b) *A* value trend

469   of THF-0, THF-GO-0.1 and THF-GO-0.2 as a function of applied hydraulic pressure (*ΔP*) to

470   the membrane lumen side to evaluate the membrane stability tested until the membrane to be

471   burst (DI water used as FS).

472

473   *3.4. Effect of pre-stabilization on PA selective layer*

474   In order to avoid membrane damage or breakage during PRO performance testing, the as-

475   spun TFC membranes were operated at maximum operating pressures (below critical pressure

476   point) set at 13.5 bar, 13.5 bar and 16.5 bar for THF-0, HHF-GO-0.1 and THF-GO-0.2,

respectively. Fig. 7 exhibits the variations of the A values of the three TFC-PRO membranes with operating time when operated under the RO mode during membrane pre-stabilization period at its maximum operating pressure. It can be seen that the A values for all membranes show a steep increase initially, and then remained stable with minor increase after about 60 min at which the yield strength of the membranes might have been reached and irreversible membrane structure begins to form while steady elongation is occurring. A schematic of PRO membrane structure variations as affected by pre-stabilization was illustrated in Fig. S7 for better understanding of membrane pre-stabilization effect on membrane structure as well as membrane performance. As can be seen from Fig. S7, during the pre-stabilization at each sample's respective pressure, both hollow fiber support and PA selective layer will be continuously expanded and compacted with time as the membrane was stabilized the applied pressure. This effect may consequently result in increase of membrane effective area attributed by the stretching and thinning of both hollow fiber support and PA layer [54]. Consequently, water transport resistance is reduced due to the decreased membrane thickness when the hydraulic stress is propagated on the membrane lumen side. Therefore, a gradual A value increase was observed for all tested samples with increase of the stabilization time as presented in Fig. 7. After pre-stabilization of TFC membranes for 1h, water permeability and salt rejection performance were evaluated at different applied pressures as shown in Fig. S8. An interesting observation is that the water permeability of TFC membranes (Fig. S8) after pre-stabilization has improved almost 3-fold from ≈ 0.3 L m^{-2} h^{-1} bar^{-1} to ≈ 0.9 L m^{-2} h^{-1} bar^{-1} at 5 bar as compared to the membranes tested without pre-stabilization (Fig. 6). However, those values were lower than that of A values revealed during pre-stabilization. These trends consequently reveal that the membranes were efficiently compacted and expanded by pre-stabilization but it was partially recovered at lower pressures due to the elastic property of polymeric membranes as described in Fig. S7. However, when the pressure increases, the water

502 permeability of membranes is again gradually increased accordingly when the pressure is

503 below their burst pressures due to the re-thinning of PA layer and re-enlargement of surface

504 area. Meanwhile, salt rejection of all tested membranes was also improved at higher applied

505 pressures (Fig. S8). This can be due to induced faster solvent permeation by reducing transport

506 resistance as a result of larger expansion and compaction of PA selective layer at higher applied

507 pressure. However, since the size of water molecules is smaller than that of salt molecules,

508 relatively larger volume of water molecules maybe transported to the permeate side than the

509 amount of salt transport as the pressure increases. Similar trend was also observed and has been

510 discussed in previous studies [9, 19, 54]. Recently, Gai et al. reported that membrane pre-

511 stabilization at a high applied pressure but slightly below their burst pressure for a certain

512 duration is an effective approach to enhance the membranes' PRO performance without

513 damaging the TFC-PRO membranes [9]. Based on the results shown in Fig. 7, we fixed the

514 membrane pre-stabilization period to be 1 h at the maximum operation pressure for each

515 membrane prior to PRO tests that were conducted to obtain the desirable PRO performance.
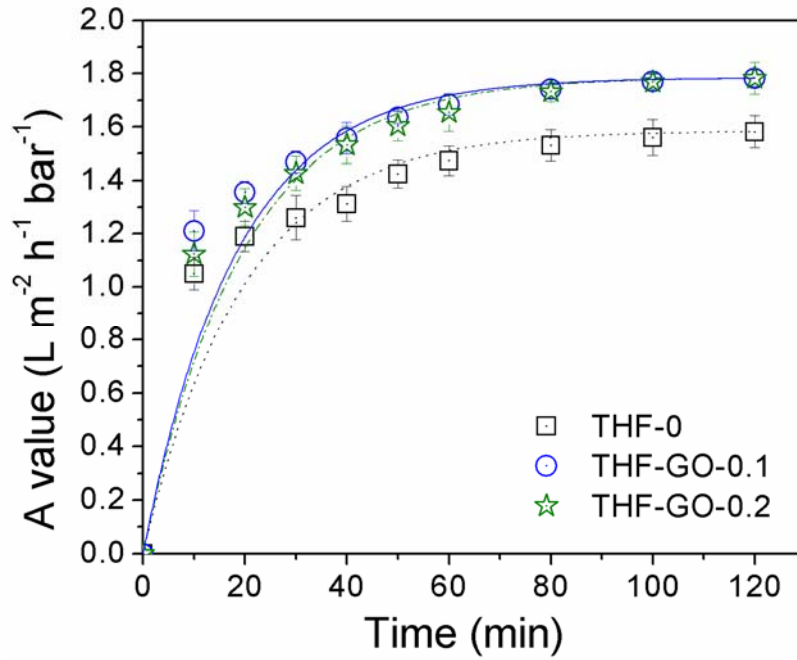
Fig. 7. *A* value trends of the TFC-PRO membranes at different applied pressures of 13.5 bar, 13.5 bar and 16.5 bar for THF-0, THF-GO-0.1 and THF-GO-0.2, respectively, as a function of time (min). The water permeability value of each points was determined with the averaged values of permeated water volume for 10 min.

3.5. Transport properties of TFC-PRO membranes

Table 3 shows the mass transport properties of the as-spun TFC-PRO hollow fiber membranes. The membranes were tested after pre-stabilization at their specified maximum operation pressures. The prepared TFC-PRO membranes had generally similar *A* values ranging from 1.22 to 1.36 L $m^{-2} h^{-1} bar^{-1}$. However, slightly improved *A* values were obtained from the THF-GO-0.1 and THF-GO-0.2. As seen from the SEM images of PA selective layer (Fig. 5), relatively thinner PA layer is formed on the GO-incorporated hollow fiber samples compared to THF-0 which might have reduced the mass transport resistance across the PA layer. Meanwhile, significant improvement of the *R* value is observed for THF-GO-0.1 (96.1%) and

THF-GO-0.2 (97.7%) compared to THF-0 with 93.4%, a trend consistent with the GO loading rate. Improved hydrophilic and porous properties of membrane surface via GO incorporation might induce the uniform distribution of MPD on the surface thus provided better environment to form a PA layer without defect, as well as thinner thickness. A similar observation was made in our previous studies which showed that a suitable GO loading in the membrane substrate can result in the most favorable condition for subsequent PA layer formation by IP process [29, 30]. The hollow fiber supports with lower surface roughness, larger pore size, and hydrophilic membrane surface induced via GO incorporation might have enhanced the PA formation for higher permeability with higher salt selectivity [29].

An additional RO experiment for TFC membranes was conducted as presented in Table S1. In order to compare their intrinsic membrane properties under similar conditions, all TFC membranes were pre-stabilized at 8 bar for 1 h before determining the intrinsic properties of the membrane. These values were then compared with the intrinsic membrane properties obtained after pre-stabilizing at their maximum pressure (slightly lower than the burst pressure). Fig. 8 shows the comparison of the A value and salt rejection properties of the TFC membranes pre-stabilized at different pressures. Both A value and salt rejection performances for TFC membranes stabilized at 8 bar revealed similar trends to those stabilized at higher pressures in the range of 13.5-16.5 bar. One of the most noticeable findings is that, both A values and salt rejection for all TFC membranes were significantly enhanced when they were pre-stabilized at higher applied pressures of 13.5-16.5 bar. When the TFC hollow fiber membranes are pre-stabilized at higher hydraulic pressures, the hollow fiber lumen may expand most likely with irreversible structural change. This may result in slightly increased membrane effective area after pre-stabilization, which then results in increased water permeability values as the same membrane area is considered for calculation of the A values. In addition, elongated elliptical

555 voids in the PA layer induced by further increased pressure may have caused higher water

556 passage while maintaining the salt selectivity [9].

557 Table 3. Intrinsic membrane properties and S values of TFC-PRO membranes.

TFC-PRO membranes	A (L m^{-2} h^{-1} bar^{-1})	B (L m^{-2} h^{-1})	B/A (bar)	R (%)	S (μm)
THF-0	1.22 ± 0.12	0.55	0.45	93.40 ± 2.55	769
THF-GO-0.1	1.36 ± 0.05	0.35	0.26	96.14 ± 1.27	577
THF-GO-0.2	1.27 ± 0.06	0.19	0.15	97.67 ± 1.19	522

558 Test conditions: Tested PRO membranes for THF-0, THF-GO-0.1 and THF-GO-0.2 were
559 conducted pre-stabilization at the pressure of 13.5 bar, 13.5 bar and 16.5 bar, respectively, for
560 1 h prior to the RO tests. Pure water permeability (A) value was determined at $\Delta P = 8$ bar with
561 the DI water as FS. The R and B values were obtained at $\Delta P = 8$ bar with the 2000 mg L^{-1} NaCl
562 as FS.

563

564
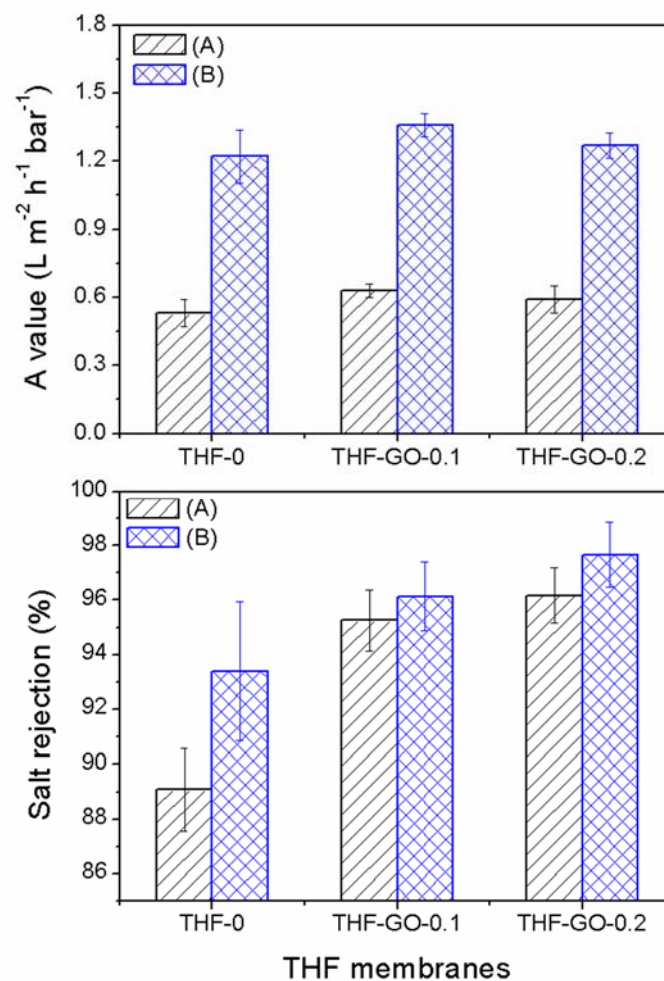
Fig. 8. A value and salt rejection performances determined at $\Delta P = 8$ bar after pre-stabilization of TFC-PRO membranes: (A) all samples were pre-stabilized at 8 bar for 1 h, (B) the samples of THF-0, THF-GO-0.1 and THF-GO-0.2 were pre-stabilized for 1 h at the pressure of 13.5 bar, 13.5 bar and 16.5 bar, respectively (DI water used as feed for A values determination and 2000 mg L^{-1} NaCl used as feed for salt rejection evaluation).

3.6. Effect of GO on TFC-PRO hollow fiber membrane performances

The PRO performance of the TFC hollow fiber membranes in terms of J_w, J_s/J_w, and W, using 1 M NaCl as DS and DI water as FS, is presented in Fig. 9. The highest J_w at ΔP=0 bar was observed for THF-GO-0.2 (43.74 L m^{-2} h^{-1}) followed by THF-GO-0.1 (42.51 L m^{-2} h^{-1}) and THF-0 (38.62 L m^{-2} h^{-1}). On the other hand, J_s/J_w of TFC-PRO membranes at ΔP=0 bar follows the order of THF-0 (0.10 g L^{-1}) > THF-GO-0.1 (0.07 g L^{-1}) > THF-GO-0.2 (0.04 g L^{-1}). These trends are mostly consistent with the intrinsic properties (A and B values) of those TFC membranes presented in Table 3. In particular, the initial J_w of the THF-GO-0.1 is lower compared to the THF-GO-0.2 membrane although its A value is higher. This is likely because of the improved hydrophilicity of the hollow fiber support at higher GO loading which significantly helped reduce the ICP effect in the membrane support layer. In addition, the S values presented in Table 3 also corresponded well with the PRO performances of the TFC membranes. The lowest S value of 522 μm was observed for THF-GO-0.2 membrane, marking the most significant improvement as compared to control membrane (THF-0, 769 μm). Several studies have observed the positive effect of hydrophilic membrane support layer in reducing the ICP effects which depend on the S values [22, 29, 30, 55-58]. Similar trends of J_w reductions were observed for all TFC membranes as hydraulic pressure increased.

588 Meanwhile, the J_s/J_w values gradually increased in the first operation (1st-run) due to the

589 expansion of the hollow fiber membrane and thinning of the PA layers. The samples THF-GO-

590 0.1 and THF-GO-0.2 showed a very stable J_s/J_w (< 0.60 g L^{-1}) at their maximum applied

591 pressures of 13.5 bar and 16.5 bar, respectively. However, as hydraulic pressure was increased,

592 relatively higher rate of J_s/J_w increment was noticed with THF-0, whose value reached 1.18 g

593 L^{-1} at 13.5 bar as shown in Fig. 9. As presented in Table 3, the lowest salt rejection and the

594 highest B/A value (0.45 bar) for THF-0 indicate the lowest separation efficiency among the

595 fabricated TFC membranes. This is a likely result of the less complete formation of PA layer

596 further accelerated the PA deformation due to stress from the hydraulic pressure. Apparently,

597 a considerable increase in J_s/J_w with pressure was observed in the second stage (2nd run) for the

598 THF-0 membrane compared to the 1st-run which is likely due to PA layer deformation under

599 repeated operation while the other membrane samples showed relatively stable or low J_s/J_w

600 values. It is interesting to note for THF-0 membrane that more J_w decrease occurred in the 2nd-

601 run than during the 1st-run and this is probably affected by the increased J_s that consequently

602 caused more severe ICP in the membrane support layer which reduces the osmotic driving

603 force across the PA selective layer [21]. However for HF-GO-0.1 membrane, relatively higher

604 J_w in the 2nd-run compared to the 1st-run was observed which might have been caused by

605 continued membrane expansion (increased effective membrane surface) with an increase in

606 operation time as well as reduced PA layer thickness with elongated free volume, but without

607 significant defects in the PA layer [9]. As comparison between THF-0 and THF-0.1 in terms

608 of mechanical stability when the same hydraulic pressure applied, therefore, it can be

609 concluded that THF-0.1 has more stable performance compared to THF-0 as it continuously

610 retained J_s/J_w as low values although more membrane expansion occurred, while significant

611 PA layer deformation appeared for THF-0. Overall, the TFC-PRO hollow fiber membrane

612 incorporated with 0.2 wt% GO exhibited the most stable PRO performance compared to other

membranes. Although HF-GO-0.2 was tested at a higher applied pressure of 16.5 bar however almost no changes in J_w and J_s/J_w were observed in the 2nd-run indicating the high stability of this PRO membrane.
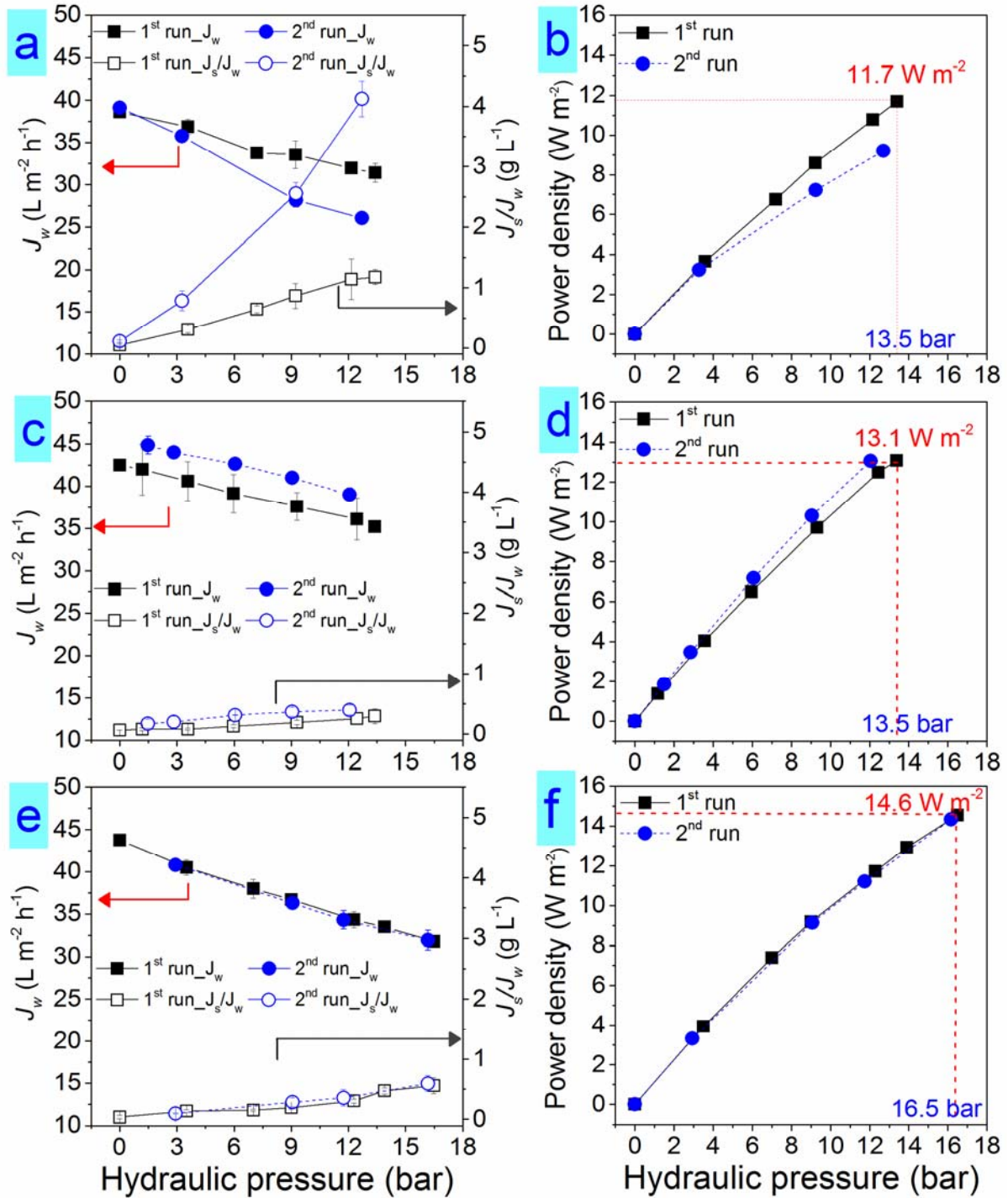
Fig. 9. Performance trends in J_w, J_s/J_w and W for THF-0 (a, b), THF-GO-0.1 (c, d), and THF-GO-0.2 (e, f) with 1 M NaCl as DS and DI water as FS, as a function of different hydraulic pressures. (The samples THF-0, THF-GO-0.1 and THF-GO-0.2 were pre-stabilized for 1 h at the pressure of 13.5 bar, 13.5 bar and 16.5 bar, respectively)

In the PRO process, a meaningful evaluation of membrane performance can be obtained by calculating the W value (W m^{-2}) of the membrane. Under the same operational pressure, PRO membrane with higher water flux can produce a higher power density as the W is proportional to J_w (Eq. (7)). From Fig. 9, the maximum W of 11.7 W m^{-2} (1st-run) at operating pressure of 13.5 bar was achieved for THF-0 membrane the power density was improved to 13.1 W m^{-2} (1st-run) by incorporating 0.1 wt% GO in the PES hollow fiber support. These results indicate that membrane substrate modified by the GO hydrophilic nanomaterial is an efficient approach for manufacturing PRO membrane for enhanced power production. The highest W of 14.6 W m^{-2} (1st-run) at 16.5 bar applied pressure was achieved with 0.2 wt% GO loading and 1 wt% increase of polymer concentration as a result of enhanced mechanical properties and water permeability, reduction of ICP effect, and achieved low S value. Nevertheless, the membrane THF-GO-0.2 showed the most stable PRO performance during the reproducibility tests (2nd-run test) among all prepared TFC membranes.

4. Conclusions

In this study, high performance TFC hollow fiber membranes were developed via incorporation of hydrophilic GO nanosheets in the PES support layer for PRO applications. The study indicated that addition of GO ($\leq$ 0.2 wt%) in the PES hollow fiber support layer

resulted in significantly improved structural morphologies as well as surface chemistry within the support layer. These results in increased overall membrane porosity with larger pore size on the surface of membrane lumen side and enhanced hydrophilicity which significantly improved water permeability without undermining the mechanical properties of the support layer. The GO incorporated hollow fiber support layer provided the most favorable lumen surface structure for the effective IP reaction producing the PA layer with higher water permeability and higher salt selectivity. The TFC-PRO hollow fiber membrane with 0.2 wt% GO incorporation in the PES support layer presented the highest J_w of 43.6 L m^{-2} h^{-1} and the lowest J_s/J_w of 0.04 g L^{-1} and significantly lower S value and ICP effects compared to the control membrane. The highest W of 14.6 W m^{-2} was achieved at 16.5 bar using 1 M NaCl as DS and DI water as FS. In this study, optimization of GO loadings in PES supports was not fully addressed, however, the effect of GO on the PRO performance indicated sufficiently from experiment results. Therefore, incorporation of controlled amount of nanomaterials such as GO nanosheets or other hydrophilic nanomaterials in hollow fiber supports could be one of the promising approaches in fabricating TFC-PRO hollow fiber membranes with enhanced PRO performance.

References

665

666

[1] J. Kim, K. Jeong, M. Park, H. Shon, J. Kim, Recent Advances in Osmotic Energy Generation via Pressure-Retarded Osmosis (PRO): A Review, Energies, 8 (2015) 11821-11845.

[2] A.P. Straub, A. Deshmukh, M. Elimelech, Pressure-retarded osmosis for power generation from salinity gradients: Is it viable?, Energy Environ. Sci., (2015).

[3] G. Han, S. Zhang, X. Li, T.-S. Chung, Progress in Pressure Retarded Osmosis (PRO) Membranes for Osmotic Power Generation, Progress in Polymer Science, (2015).

[4] A. Achilli, A.E. Childress, Pressure retarded osmosis: From the vision of Sidney Loeb to the first prototype installation — Review, Desalination, 261 (2010) 205-211.

[5] G.D. Mehta, S. Loeb, Internal polarization in the porous substructure of a semipermeable membrane under pressure-retarded osmosis, Journal of Membrane Science, 4 (1978) 261-265.

[6] N.Y. Yip, M. Elimelech, Comparison of energy efficiency and power density in pressure retarded osmosis and reverse electrodialysis, Environmental science & technology, 48 (2014) 11002-11012.

[7] G. Han, S. Zhang, X. Li, T.-S. Chung, Progress in pressure retarded osmosis (PRO) membranes for osmotic power generation, Progress in Polymer Science, 51 (2015) 1-27.

[8] S. Zhang, P. Sukitpaneenit, T.-S. Chung, Design of robust hollow fiber membranes with high power density for osmotic energy production, Chemical Engineering Journal, 241 (2014) 457-465.

[9] W. Gai, X. Li, J.Y. Xiong, C.F. Wan, T.-S. Chung, Evolution of micro-deformation in inner-selective thin film composite hollow fiber membranes and its implications for osmotic power generation, Journal of Membrane Science, 516 (2016) 104-112.

[10] N.Y. Yip, A. Tiraferri, W.A. Phillip, J.D. Schiffman, L.A. Hoover, Y.C. Kim, M. Elimelech, Thin-film composite pressure retarded osmosis membranes for sustainable power

690 generation from salinity gradients, Environmental Science & Technology, 45 (2011) 4360-
691 4369.

692 [11] S. Chou, R. Wang, L. Shi, Q. She, C. Tang, A.G. Fane, Thin-film composite hollow fiber
693 membranes for pressure retarded osmosis (PRO) process with high power density, Journal of
694 Membrane Science, 389 (2012) 25-33.

695 [12] M. Tian, R. Wang, K. Goh, Y. Liao, A.G. Fane, Synthesis and characterization of high-
696 performance novel thin film nanocomposite PRO membranes with tiered nanofiber support
697 reinforced by functionalized carbon nanotubes, Journal of Membrane Science, 486 (2015) 151-
698 160.

699 [13] X. Song, Z. Liu, D.D. Sun, Energy recovery from concentrated seawater brine by thin-
700 film nanofiber composite pressure retarded osmosis membranes with high power density,
701 Energy & Environmental Science, 6 (2013) 1199.

702 [14] G. Han, S. Zhang, X. Li, T.-S. Chung, High performance thin film composite pressure
703 retarded osmosis (PRO) membranes for renewable salinity-gradient energy generation, Journal
704 of Membrane Science, 440 (2013) 108-121.

705 [15] N.Y. Yip, A. Tiraferri, W.A. Phillip, J.D. Schiffman, L.A. Hoover, Y.C. Kim, M.
706 Elimelech, Thin-film composite pressure retarded osmosis membranes for sustainable power
707 generation from salinity gradients, Environmental science & technology, 45 (2011) 4360-4369.

708 [16] S. Lim, M.J. Park, S. Phuntsho, A. Mai-Prochnow, A.B. Murphy, D. Seo, H. Shon, Dual-
709 layered nanocomposite membrane incorporating graphene oxide and halloysite nanotube for
710 high osmotic power density and fouling resistance, Journal of Membrane Science, 564 (2018)
711 382-393.

712 [17] R.R. Gonzales, M.J. Park, T.-H. Bae, Y. Yang, A. Abdel-Wahab, S. Phuntsho, H.K. Shon,
713 Melamine-based covalent organic framework-incorporated thin film nanocomposite
714 membrane for enhanced osmotic power generation, Desalination, 459 (2019) 10-19.

715 [18] G. Han, P. Wang, T.S. Chung, Highly robust thin-film composite pressure retarded
716 osmosis (PRO) hollow fiber membranes with high power densities for renewable salinity-
717 gradient energy generation, Environmental science & technology, 47 (2013) 8070-8077.

718 [19] S. Chou, R. Wang, A.G. Fane, Robust and High performance hollow fiber membranes for
719 energy harvesting from salinity gradients by pressure retarded osmosis, Journal of Membrane
720 Science, 448 (2013) 44-54.

721 [20] S.P. Sun, T.S. Chung, Outer-selective pressure-retarded osmosis hollow fiber membranes
722 from vacuum-assisted interfacial polymerization for osmotic power generation, Environmental
723 science & technology, 47 (2013) 13167-13174.

724 [21] G. Han, T.-S. Chung, Robust and high performance pressure retarded osmosis hollow fiber
725 membranes for osmotic power generation, AIChE Journal, 60 (2014) 1107-1119.

726 [22] P.G. Ingole, W. Choi, K.H. Kim, C.H. Park, W.K. Choi, H.K. Lee, Synthesis,
727 characterization and surface modification of PES hollow fiber membrane support with
728 polydopamine and thin film composite for energy generation, Chemical Engineering Journal,
729 243 (2014) 137-146.

730 [23] X. Li, T.-S. Chung, Thin-film composite P84 co-polyimide hollow fiber membranes for
731 osmotic power generation, Applied Energy, 114 (2014) 600-610.

732 [24] F.-J. Fu, S. Zhang, T.-S. Chung, Sandwich-structured hollow fiber membranes for osmotic
733 power generation, Desalination, 376 (2015) 73-81.

734 [25] Y.C. Kim, M. Elimelech, Adverse impact of feed channel spacers on the performance of
735 pressure retarded osmosis, Environmental science & technology, 46 (2012) 4673-4681.

736 [26] W.R. Thelin, E. Sivertsen, T. Holt, G. Brekke, Natural organic matter fouling in pressure
737 retarded osmosis, Journal of Membrane Science, 438 (2013) 46-56.

738 [27] S. Chou, R. Wang, L. Shi, Q. She, C. Tang, A.G. Fane, Thin-film composite hollow fiber
739 membranes for pressure retarded osmosis (PRO) process with high power density, Journal of
740 Membrane Science, 389 (2012) 25-33.

741 [28] F.-J. Fu, S. Zhang, S.-P. Sun, K.-Y. Wang, T.-S. Chung, POSS-containing delamination-
742 free dual-layer hollow fiber membranes for forward osmosis and osmotic power generation,
743 Journal of Membrane Science, 443 (2013) 144-155.

744 [29] M.J. Park, S. Phuntsho, T. He, G.M. Nisola, L.D. Tijing, X.-M. Li, G. Chen, W.-J. Chung,
745 H.K. Shon, Graphene oxide incorporated polysulfone substrate for the fabrication of flat-sheet
746 thin-film composite forward osmosis membranes, Journal of Membrane Science, 493 (2015)
747 496-507.

748 [30] S. Lim, M.J. Park, S. Phuntsho, L.D. Tijing, G.M. Nisola, W.-G. Shim, W.-J. Chung, H.K.
749 Shon, Dual-layered nanocomposite substrate membrane based on polysulfone/graphene oxide
750 for mitigating internal concentration polarization in forward osmosis, Polymer, 110 (2017) 36-
751 48.

752 [31] M. Hu, B. Mi, Enabling graphene oxide nanosheets as water separation membranes,
753 Environmental science & technology, 47 (2013) 3715-3723.

754 [32] J. Lee, H.-R. Chae, Y.J. Won, K. Lee, C.-H. Lee, H.H. Lee, I.-C. Kim, J.-m. Lee, Graphene
755 oxide nanoplatelets composite membrane with hydrophilic and antifouling properties for
756 wastewater treatment, Journal of Membrane Science, 448 (2013) 223-230.

757 [33] B. Mi, Graphene Oxide Membranes for Ionic and Molecular Sieving, Science, 343 (2014)
758 740-742.

759 [34] F. Perreault, M.E. Tousley, M. Elimelech, Thin-Film Composite Polyamide Membranes
760 Functionalized with Biocidal Graphene Oxide Nanosheets, Environmental Science &
761 Technology Letters, 1 (2014) 71-76.

762 [35] S. Stankovich, D.A. Dikin, G.H. Dommett, K.M. Kohlhaas, E.J. Zimney, E.A. Stach, R.D.
763 Piner, S.T. Nguyen, R.S. Ruoff, Graphene-based composite materials, Nature, 442 (2006) 282-
764 286.

765 [36] W.S. Hummers, R.E. Offeman, Preparation of Graphitic Oxide, National Lead Company,
766 (1958).

767 [37] A.M. Dimiev, J.M. Tour, Mechanism of Graphene Oxide Formation, ACS NANO, 8 (2014)
768 3060-3068.

769 [38] Y. Ji, X.-M. Li, Y. Yin, Y.-Y. Zhang, Z.-W. Wang, T. He, Morphological control and
770 cross-flow filtration of microfiltration membranes prepared via a sacrificial-layer approach,
771 Journal of Membrane Science, 353 (2010) 159-168.

772 [39] X.M. Li, Y. Ji, T. He, M. Wessling, A sacrificial-layer approach to prepare microfiltration
773 membranes, Journal of Membrane Science, 320 (2008) 1-7.

774 [40] T. He, M.H.V. Mulder, H. Strathmann, M. Wessling, Preparation of composite hollow
775 fiber membranes: co-extrusion of hydrophilic coatings onto porous hydrophobic support
776 structures, Journal of Membrane Science, 207 (2002) 143-156.

777 [41] T. He, M.H.V. Mulder, M. Wessling, Preparation of porous hollow fiber membranes with
778 a triple-orifice spinneret, Journal of Applied Polymer Science, 87 (2003) 2151-2157.

779 [42] J.Y. Xiong, Z.L. Cheng, C.F. Wan, S.C. Chen, T.-S. Chung, Analysis of flux reduction
780 behaviors of PRO hollow fiber membranes: Experiments, mechanisms, and implications,
781 Journal of Membrane Science, 505 (2016) 1-14.

782 [43] P. Sukitpaneenit, T.S. Chung, High performance thin-film composite forward osmosis
783 hollow fiber membranes with macrovoid-free and highly porous structure for sustainable water
784 production, Environmental science & technology, 46 (2012) 7358-7365.

785 [44] S. Zinadini, A.A. Zinatizadeh, M. Rahimi, V. Vatanpour, H. Zangeneh, Preparation of a
786 novel antifouling mixed matrix PES membrane by embedding graphene oxide nanoplates,
787 Journal of Membrane Science, 453 (2014) 292-301.

788 [45] A.K. Shukla, J. Alam, M. Alhoshan, L.A. Dass, M.R. Muthumareeswaran, Development
789 of a nanocomposite ultrafiltration membrane based on polyphenylsulfone blended with
790 graphene oxide, Scientific reports, 7 (2017) 41976.

791 [46] Y. Wang, R. Ou, H. Wang, T. Xu, Graphene oxide modified graphitic carbon nitride as a

792 modifier for thin film composite forward osmosis membrane, Journal of Membrane Science,

793 475 (2015) 281-289.

794 [47] H. Zhao, L. Wu, Z. Zhou, L. Zhang, H. Chen, Improving the antifouling property of

795 polysulfone ultrafiltration membrane by incorporation of isocyanate-treated graphene oxide,

796 Physical chemistry chemical physics : PCCP, 15 (2013) 9084-9092.

797 [48] D. Qin, Z. Liu, D. Delai Sun, X. Song, H. Bai, A new nanocomposite forward osmosis

798 membrane custom-designed for treating shale gas wastewater, Scientific reports, 5 (2015)

799 14530.

800 [49] C. Zhao, X. Xu, J. Chen, F. Yang, Effect of graphene oxide concentration on the

801 morphologies and antifouling properties of PVDF ultrafiltration membranes, Journal of

802 Environmental Chemical Engineering, 1 (2013) 349-354.

803 [50] W. Yan, Z. Wang, J. Wu, S. Zhao, J. Wang, S. Wang, Enhancing the flux of brackish

804 water TFC RO membrane by improving support surface porosity via a secondary pore-forming

805 method, Journal of Membrane Science, 498 (2016) 227-241.

806 [51] J. Ren, M.R. Chowdhury, J. Qi, L. Xia, B.D. Huey, J.R. McCutcheon, Relating osmotic

807 performance of thin film composite hollow fiber membranes to support layer surface pore size,

808 Journal of Membrane Science, 540 (2017) 344-353.

809 [52] H. Yan, X. Miao, J. Xu, G. Pan, Y. Zhang, Y. Shi, M. Guo, Y. Liu, The porous structure

810 of the fully-aromatic polyamide film in reverse osmosis membranes, Journal of Membrane

811 Science, 475 (2015) 504-510.

812 [53] W.C.L. Lay, J. Zhang, C. Tang, R. Wang, Y. Liu, A.G. Fane, Factors affecting flux

813 performance of forward osmosis systems, Journal of Membrane Science, 394-395 (2012) 151-

814 168.

815 [54] Y. Chen, L. Setiawan, S. Chou, X. Hu, R. Wang, Identification of safe and stable operation

816 conditions for pressure retarded osmosis with high performance hollow fiber membrane,

817 Journal of Membrane Science, 503 (2016) 90-100.

818   [55] M.J. Park, R.R. Gonzales, A. Abdel-Wahab, S. Phuntsho, H.K. Shon, Hydrophilic

819   polyvinyl alcohol coating on hydrophobic electrospun nanofiber membrane for high

820   performance thin film composite forward osmosis membrane, Desalination, 426 (2018) 50-59.

821   [56] S. Sahebi, S. Phuntsho, Y.C. Woo, M.J. Park, L.D. Tijing, S. Hong, H.K. Shon, Effect of

822   sulphonated polyethersulfone substrate for thin film composite forward osmosis membrane,

823   Desalination, 389 (2016) 129-136.

824   [57] J.T. Arena, B. McCloskey, B.D. Freeman, J.R. McCutcheon, Surface modification of thin

825   film composite membrane support layers with polydopamine: Enabling use of reverse osmosis

826   membranes in pressure retarded osmosis, Journal of Membrane Science, 375 (2011) 55-62.

827   [58] R.R. Gonzales, J.M. Park, L. Tijing, S.D. Han, S. Phuntsho, K.H. Shon, Modification of

828   nanofiber support layer for thin film composite forward osmosis membranes via layer-by-layer

829   polyelectrolyte deposition, Membranes, 8 (2018).

830